

Structural Signatures of Ultrastability in a Deposited Glassformer

Fabio Leoni^{1,*}, Fausto Martelli², C. Patrick Royall^{3,4,5,6} and John Russo¹

¹*Dipartimento di Fisica, Università degli Studi di Roma La Sapienza, Piazzale Aldo Moro 5, Rome 00185, Italy*

²*IBM Research Europe, Hartree Centre, Daresbury WA4 4AD, United Kingdom*

³*Gulliver UMR CNRS 7083, ESPCI Paris, Université PSL, 75005 Paris, France*

⁴*School of Chemistry, Cantock's Close, University of Bristol, Bristol BS8 1TS, United Kingdom*

⁵*Centre for Nanoscience and Quantum Information, Tyndall Avenue, Bristol BS8 1FD, United Kingdom*

⁶*H. H. Wills Physics Laboratory, Tyndall Avenue, Bristol BS8 1TL, United Kingdom*



(Received 14 November 2022; accepted 13 April 2023; published 12 May 2023)

Glasses obtained from vapor deposition on a cold substrate have superior thermodynamic and kinetic stability with respect to ordinary glasses. Here we perform molecular dynamics simulations of vapor deposition of a model glassformer and investigate the origin of its high stability compared to that of ordinary glasses. We find that the vapor deposited glass is characterized by locally favored structures (LFSs) whose occurrence correlates with its stability, reaching a maximum at the optimal deposition temperature. The formation of LFSs is enhanced near the free surface, hence supporting the idea that the stability of vapor deposited glasses is connected to the relaxation dynamics at the surface.

DOI: [10.1103/PhysRevLett.130.198201](https://doi.org/10.1103/PhysRevLett.130.198201)

The formation of glass films obtained from vapor deposition on a substrate is attracting ever increasing attention in the scientific community due to its technological and theoretical implications [1–4]. Vapor deposited glasses (DGs) obtained at specific conditions can show remarkable properties [5], which for a conventional glass (e.g., obtained by quenching of a liquid melt) would require thousands of years of aging [6]. These glasses are called ultrastable glasses (USGs) and are obtained by careful consideration of the substrate temperature (T_{sub}) kept below the glass transition temperature (T_g) and of the deposition rate γ_{DG} [1,5,7–11]. While conventional glasses show low mechanical stability, which results in spontaneous aging and devitrification over time [12], leading to structural changes during its lifetime in many applications, USGs exhibit enhanced kinetic and thermodynamic stability with respect to them. Understanding these properties has the potential to bring fundamental insights into the nature of deeply supercooled liquids and structural properties of amorphous solids from one side and to provide new routes for engineering materials with specific properties from the other side, for example, in the realization of organic light-emitting diode displays [1], in the stabilization of amorphous pharmaceuticals [1], in the miniaturization of next-generation computing components and interconnect technologies [13–17], or in improving coatings and design of composite materials using metallic glasses [11,18,19].

The enhanced properties of USGs with respect to conventional glasses originate from structural configurations corresponding to deeper minima in the potential energy landscape (PEL) [20]. The PEL is strictly related

to dynamical, thermodynamic, structural, and chemical properties of amorphous materials [1,21,22].

Experiments [5,23,24], simulations [6,10,25], and theory [26] suggest that the key to understand the formation of USGs by vapor deposition is the enhanced mobility at the surface of the deposited layer, which correlates with the stability of the glass. Indeed, it is estimated [5] that, up to temperatures far below T_g , molecules at the surface remain mobile for several bulk relaxation times during which, for suitable control parameters, they find near-equilibrium configurations before being buried by other molecules undergoing deposition. However, it remains unclear how exactly the enhanced mobility at the surface plays its role in the formation of ultrastable deposited glasses [27].

A relevant question is whether the glasses produced by vapor deposition share the same structural properties of glasses obtained by cooling [25]. While long range properties can be inferred from two-point correlation functions [28–30], investigation of short range structures is very limited [31–33]. Instead, different higher order methods have been developed for this purpose [34]. Recently, bond-orientational order parameters have uncovered a link between liquid and glassy water [35] and, together with Voronoi polyhedra, have been correlated to the stability of deposited glasses [36], while nontrivial symmetries have been found in glassy water adopting a generic approach [37,38]. In this Letter, we follow Ref. [39] and refer to icosahedral motifs as locally favored structures (LFSs). A strong correlation between the number of LFSs and temperature or packing fraction has been found in systems as different as colloids [40,41] and metallic glasses [36,42]. In particular, previous studies on deposited glasses have

found correlations between global (averaged over space) descriptors associated with the full sample and its stability [25,36,43], whereas here, in addition to the global structural characterization through the system density (see Fig. 2), we perform a local characterization through LFSs that can be correlated to spatially dependent properties of the sample, such as its mobility profile (see Figs. S6 and S7 [44]).

To understand the connection between the stability of deposited glasses and their structural properties, here we numerically investigate the process of formation of a model metallic glassformer for which the LFSs in equilibrium have been thoroughly investigated. The study of metallic glassformers is of great interest also from the experimental point of view for the unique mechanical and functional properties that these materials possess [18,19].

We adopt the Wahnström (WAhN) model [48], which is composed of an equimolar additive bidisperse Lennard-Jones mixture (see Supplemental Material [44]). Several studies [39,48–51] have shown that for this system the LFSs consist of particles arranged in the icosahedral geometry. This model thus allows us to directly correlate the thermodynamic properties of the glass with the fraction of LFSs and investigate the connection between glasses prepared via different routes.

We study the system by performing molecular dynamics simulations (using LAMMPS [52]). The units of energy, length, and time are ϵ , σ , and $t^* = (m_1\sigma^2/\epsilon)^{1/2}$, respectively. The integration time step is set to 0.005. Quantities are expressed in these reduced units. We first estimate the glass transition temperature in the bulk. Glasses prepared in the presence of a free surface equilibrate at ambient pressure and for which we obtain $T_g \simeq 0.36$ (see Supplemental Material [44]).

We compare both structural and dynamical properties of the DG with that of a conventional quenched glass (QG). The DG is obtained, similar to Refs. [6,10], by injecting a particle from a random position along x and y at the top of the simulation box with a frequency described by the deposition rate γ_{DG} up to deposit a total of $N = 4000$ particles, i.e., 2000 of type 1 and 2000 of type 2 (see Fig. 1). γ_{DG} is given by the ratio between the thickness of the deposited layer and the elapsed time: $\gamma_{\text{DG}} = \Delta z / \Delta t$. We inject one particle every 5×10^4 integration steps, so that we obtain $\gamma_{\text{DG}} \simeq 10^{-7} \sigma / dt = 2 \times 10^{-5}$. The substrate (see Fig. 1) placed at the bottom of the simulation box, periodic in x and y , is composed of a disordered WAhN mixture with 250 particles of type 1 and 250 of type 2 at a number density in reduced units equal to $\rho^* = \rho(\sigma)^3 = 0.75$, forming a layer of thickness $\sim 3\sigma$ and kept at temperature T_{sub} (NVT ensemble, see Supplemental Material [44]).

To prepare the QG with the same boundary conditions as the DG, we melt the DG by instantaneously heating it up to $T = 1$, let the system equilibrate for a time of 5×10^3 , and then cool it down to $T = 0.1$ at cooling rate γ_{QG} . In doing so, we keep the substrate in contact with the deposited

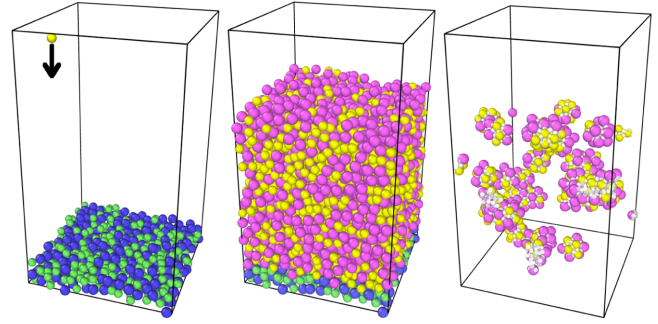


FIG. 1. Snapshots showing for $T = 0.42$ (left) the substrate formed by particles of type 1 (green) and 2 (blue) with the injection of a type 1 (yellow) particle, and (center) the deposited layer formed by particle of type 1 (yellow) and 2 (magenta). (Right) Particles belonging to icosahedra are shown. The snapshots are made with OVITO [53].

layer. The two cooling protocols we consider go from $T = 1$ to $T = 0.1$ in a time of 5×10^6 and 5×10^4 , which correspond to $\gamma_{\text{QG}} = 1.8 \times 10^{-7}$ and 1.8×10^{-5} , respectively. To convert reduced units in real numbers, we consider type 1 particles to be an argon atom with $\epsilon/k_B = 120$ K, where k_B is the Boltzmann constant, and $t^* = 2.2$ ps [51], such that $\gamma_{\text{QG}} \sim 0.01$ and $\gamma_{\text{QG}} \sim 1$ K/ns, respectively. We choose a deposition rate such that the length of the simulations for DG (in a time of 10^6) is intermediate between the QG cooling times. In this way, we can compare the structure of the as-deposited layer (immediately after deposition has finished) with that of quenched glasses that have had comparable relaxation times. All the structural and dynamical properties that we consider are computed in the core of the deposited and quenched layer, unless otherwise specified. The core is defined as the part of the layer where particles have coordinates $z_{\text{bot}} + 4\sigma < z < z_{\text{top}} - 4\sigma$, with z_{bot} , z_{top} as the bottom and top edges of the layer, respectively (see Supplemental Material [44], which includes Ref. [45]). Among the different ways to quantify the stability of glasses [2,43,54–57], we compute the core internal potential energy u_{core} and density ρ_{core} . Here we show (Fig. 2 and left-top inset therein) u_{core} and ρ_{core} versus T for the deposited and quenched glasses at different cooling rates. In the right-bottom inset of Fig. 2, we show both the opposite of the internal potential energy per particle difference Δu_{core} (also shown in Fig. S8 [44]) and density difference $\Delta \rho_{\text{core}}$ between DG and QG for both γ_{QG} . From it we obtain that the optimal temperature of the substrate to get a stable deposited glass falls in the range $T \in [0.32, 0.42]$.

The LFSs in the Wahnström model is the icosahedron [48–50]. To identify LFSs, we use the topological cluster classification (TCC) algorithm [49]. In Fig. 3, we show the average population of icosahedral clusters at different temperatures for DG (red squares) and QG at two cooling

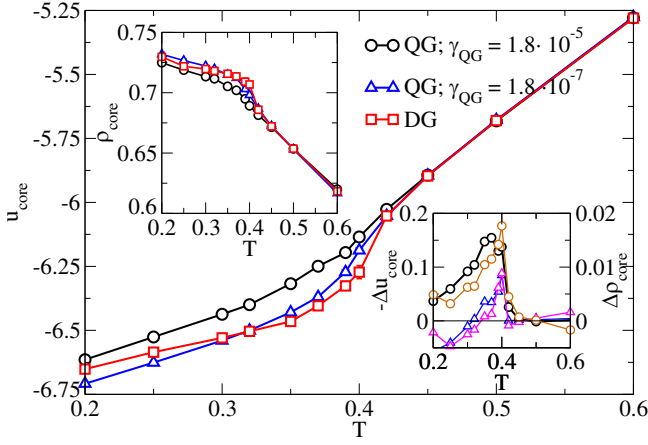


FIG. 2. Potential energy per particle u_{core} versus temperature T for the DG and QG at annealing rates $\gamma_{\text{QG}} = 1.8 \times 10^{-5}$, 1.8×10^{-7} . Left-top inset: density versus temperature associated with the core of the DG and QG. Right-bottom inset: u_{core} difference between QG and DG (black circles and blue triangles), and ρ_{core} difference between DG and QG (brown circles and magenta triangles) for $\gamma_{\text{QG}} = 1.8 \times 10^{-5}$ and 1.8×10^{-7} , respectively.

rates (black circles and blue upward triangles) and the equilibrated bulk at zero pressure (green downward triangles, down to the temperature where we can achieve equilibration). Interestingly, the deposited layer shows a peak in the distribution of icosahedra in the range of temperatures 0.32–0.36 (corresponding to a fraction of T_g in the range 0.85–1), while annealed glasses show a continuous increase in the concentration of icosahedra for decreasing temperature for all cooling rates simulated. Despite the energy and density curves of the slow QGs and DGs being very close in this region, the analysis of LFSs shows a clear difference between the two glasses and an increased stability of DG in a window of temperatures around T_g . Moreover, compared to QG with its monotonic temperature dependence, the DG has an excess of LFSs only in this temperature range, showing that the effectiveness of vapor deposition depends on optimal glass forming conditions. Comparing to the bulk $P = 0$ simulations (green downward triangle points), we see that DG follows the equilibrium curve much closer than the QG samples. We thus find that the DGs are characterized by the same LFSs as the equilibrium case, being structurally equivalent to QG glasses before they fall out of equilibrium. For larger values of γ_{DG} , we did not observe any relevant shift in the temperature location of the peak of $\langle N_c/N \rangle$. The main features of the glasses obtained from Fig. 3 do not change if, instead of the core of the layer, different regions are considered (see Supplemental Material [44]).

We verified that also for another popular glassformer [the Kob-Andersen (KA) model [58]] the deposited layer shows a peak in the distribution of the relevant LFSs around an optimal temperature (see Supplemental Material [44]).

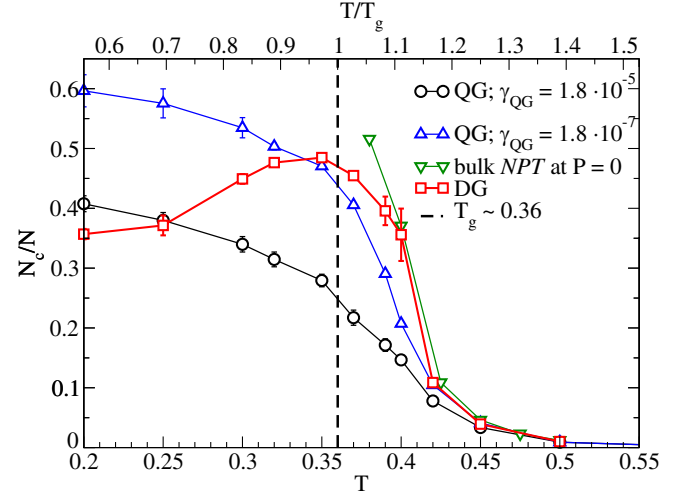


FIG. 3. Fraction of particles detected within icosahedra with the TCC algorithm for DG (red squares), QG at two cooling rates (black circles and blue upward triangles), and equilibrated bulk at zero pressure (green downward triangles).

While icosahedra capture short range order, Frank-Kasper (FK) polyhedra [51,59] allow one to reveal the possible crystallization of the system into MgZn_2 -like structures (given by a tetrahedral network of FK bonds). A FK analysis shows that these bonds are disordered, and so no crystallization happens at the conditions considered in this Letter; the number of bonds follows a similar behavior to that of Fig. 3 (see Supplemental Material [44]). We verified that, unlike molecular glasses made of anisotropic constituents [1], the two-point correlation functions along different directions of DGs and QGs, which are made of isotropic constituents, are isotropic (see Fig. S4 [44]), as observed also for the KA model in Ref. [36].

In the upper panel of Fig. 4, we show the average density profile $\langle \rho_c \rangle$ of the fraction of particles detected within icosahedra as a function of the distance from the free surface d_s for the as-deposited DG and the QG at $\gamma_{\text{QG}} = 1.8 \times 10^{-7}$, while in the lower panel, we show the respective average number density profile $\langle \rho \rangle$. At high temperature ($T = 0.42$), the DG and QG show a similar, flat icosahedra profile, which mirrors the density profile, as expected at liquid-vapor interfaces [60]. Decreasing temperature, the QG develops an increasingly pronounced peak in ρ_c at a distance from the free surface $4 \lesssim d_s \lesssim 5$ (range marked with a vertical bar in Fig. 4) and an overall increasing LFS density. On the other hand, when decreasing temperature, the DG shows a peak at $13 \lesssim d_s \lesssim 16$, while further decreasing temperature (below T_g) another peak develops at $4 \lesssim d_s \lesssim 5$. The overall LFS density of the DG reaches a maximum around the temperature corresponding to the peak in the fraction of icosahedra (see Fig. 3). The behavior of the QG confirms the role of the free surface to enhance the formation of LFSs (up to a distance $\sim 7\sigma$ from it) compared to the bulk. This same mechanism

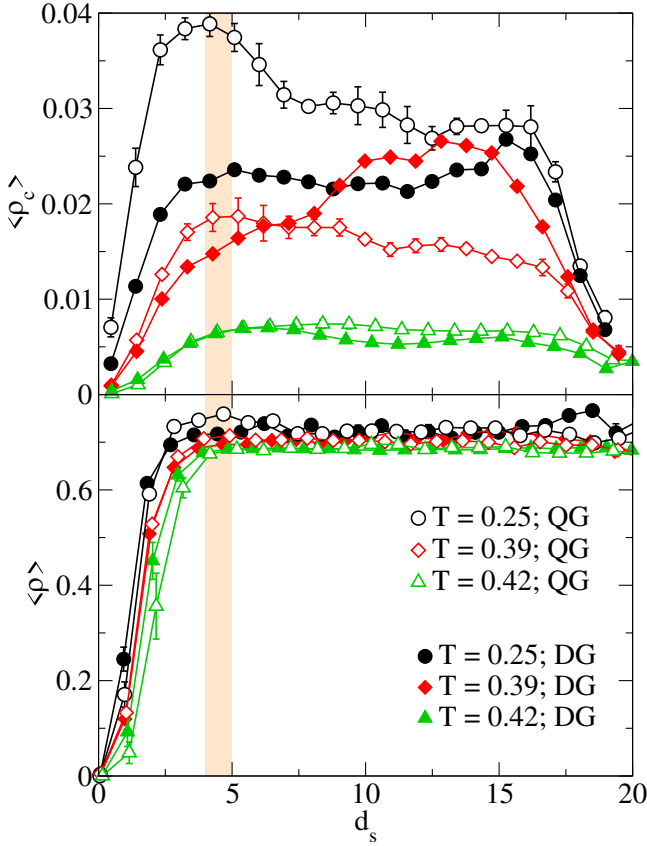


FIG. 4. Upper: average density profile $\langle \rho_c \rangle$ of the fraction of particles detected within icosahedra as a function of the distance from the free surface d_s . Lower: density profiles $\langle \rho \rangle$ versus d_s .

explains the behavior of the DG seen in Fig. 4: all particles of the as-deposited layer at some point during the deposition process were located at or near the free surface, and consequently, the concentration of LFSs underneath the surface was enhanced. However, with decreasing temperature, the mobility near the free surface decreases (see Fig. S6 [44]), so reducing the time available to particles near the free surface to find local stable configurations before getting buried by other particles undergoing deposition.

These results support the idea that the enhanced stability of vapor deposited glasses can be attributed to the faster relaxation of the surface [61], which allows the formation of LFSs for several layers below the surface. While the density profile is monotonic (inset of Fig. 4), the presence of peaks in the LFS profiles of Fig. 4 shows that the surface enhances the formation of local structures compared to the bulk.

In Fig. 5, we show the structural relaxation time τ_α and the Vogel-Fulcher-Tammann (VFT) fit for the bulk simulations at $P = 0$ (green downward triangles), together with the DG and the QG at both cooling rates for $T = 0.37$, above T_g , but close to the maximum in the number of LFSs (see Fig. 3). Relaxation times are obtained by fitting the self-intermediate scattering functions with the Kolrausch-Williams-Watts law (see Supplemental Material [44],

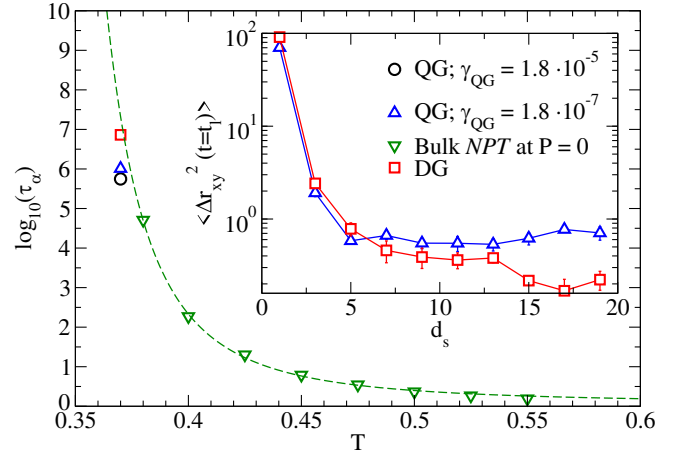


FIG. 5. Structural relaxation time versus temperature for the bulk at $P = 0$ (green triangles) fitted with the VFT law (dashed line, see Supplemental Material [44]). The DG (red square) and QG at $\gamma_{QG} = 1.8 \times 10^{-5}$ (black circle) and $\gamma_{QG} = 1.8 \times 10^{-7}$ (blue triangle) are shown for $T = 0.37$. Inset: MSD in the xy plane at the lag time $t_l = 2 \times 10^3$ as a function of the distance from the free surface d_s at $T = 0.37$.

which includes Refs. [46,47]) after the deposition or quenching process has ended. The figure shows that the DG (at the state point where LFSs are close to the maximum) has a relaxation time closer to the bulk equilibrium extrapolated value (green dashed line) compared to the QG. The correspondence between the maximum in LFSs (Fig. 3) and the longest relaxation time (Fig. 5), and its closeness to the equilibrium extrapolated value, shows once more that vapor deposition produces samples that are the closest to their bulk equilibrium counterparts and are considerably more aged than QGs. In the inset of Fig. 5, we compare the 2D mean square displacement (MSD) along the xy plane at the lag time $t_l = 2 \times 10^3$ as a function of the distance from the free surface d_s of the DG with the QG at $\gamma_{QG} = 1.8 \times 10^{-7}$. Similar to Ref. [62], particles within the first $\sim 5\sigma$ layers underneath the free surface remain from 1 to almost 3 orders of magnitude faster than particles deep inside the layer, even at low T . Furthermore, the MSD correlates with the stability of the glass (see Fig. S6 [44]) and with the local structural classification (icosahedra are slower, see Fig. S7 [44]).

In conclusion, we have investigated the formation of a glass from vapor deposition for a well-known model glassformer (Wahnström mixture) for which the locally favored structure is known and corresponds to icosahedral environments. This has allowed us to investigate the relation between glass stability and local structure formation, finding a close link between them. In particular, despite bulk quantities like energy and density being very similar between deposited and quenched glasses, the optimal deposition temperature occurs in correspondence to a peak in the fraction of LFSs (Fig. 3). Here, both structure and

structural relaxation lie close to the extrapolated equilibrium value (obtained from bulk simulations at $P = 0$), reinforcing the idea that the DG shares the same microscopic properties of well-aged glasses. We also investigated the role of the free surface in the formation of ultrastable glasses, showing that at optimal deposition conditions the mobility profile along the deposition direction, enhanced at the surface and suppressed in the bulk, is correlated with the stability of the glass through the formation of an excess of LFSs up to several layers below the surface.

F. L. and J. R. acknowledge support from the European Research Council Grant No. DLV-759187 and CINECA-ISCRA for HPC resources. C. P. R. acknowledges funding through the ANR Grant DiViNew.

*Corresponding author.

fabio.leoni@uniroma1.it

- [1] M. D. Ediger, *J. Chem. Phys.* **147**, 210901 (2017).
- [2] C. Rodriguez-Tinoco, M. Gonzalez-Silveira, M. A. Ramos *et al.*, *Riv. Nuovo Cim.* **45**, 325 (2022).
- [3] S. Rosnagel, *J. Vac. Sci. Technol. A* **21**, S74 (2003).
- [4] S. Rosnagel, *IBM J. Res. Dev.* **43**, 163 (1999).
- [5] S. F. Swallen, K. L. Kearns, M. K. Mapes, Y. S. Kim, R. J. McMahon, M. D. Ediger, T. Wu, L. Yu, and S. Satija, *Science* **315**, 353 (2007).
- [6] I. Lyubimov, M. D. Ediger, and J. J. de Pablo, *J. Chem. Phys.* **139**, 144505 (2013).
- [7] S. L. L. M. Ramos, M. Oguni, K. Ishii, and H. Nakayama, *J. Phys. Chem. B* **115**, 14327 (2011).
- [8] K. L. Kearns, S. F. Swallen, M. D. Ediger, T. Wu, and L. Yu, *J. Chem. Phys.* **127**, 154702 (2007).
- [9] E. León-Gutiérrez, G. García, A. F. Lopeandía, J. Fraxedas, M. T. Clavaguera-Mora, and J. Rodríguez-Viejo, *J. Chem. Phys.* **129**, 181101 (2008).
- [10] L. Berthier, P. Charbonneau, E. Flenner, and F. Zamponi, *Phys. Rev. Lett.* **119**, 188002 (2017).
- [11] P. Luo, C. Cao, F. Zhu, Y. Lv, Y. Liu, P. Wen, H. Bai, G. Vaughan, M. Di Michiel, B. Ruta *et al.*, *Nat. Commun.* **9**, 1389 (2018).
- [12] C. A. Angell, K. L. Ngai, G. B. McKenna, P. F. McMillan, and S. W. Martin, *J. Appl. Phys.* **88**, 3113 (2000).
- [13] A. Simon, O. van der Straten, N. A. Lanzillo, C.-C. Yang, T. Nogami, and D. C. Edelstein, *J. Vac. Sci. Technol. A* **38**, 053402 (2020).
- [14] D. Sil, Y. Sulehria, O. Gluschenkov, T. Nogami, R. Cornell, A. Simon, J. Li, J. Demarest, B. Haran, C. Lavoie *et al.*, in *Proceedings of the 2021 IEEE International Interconnect Technology Conference (IITC)* (IEEE, Piscataway, NJ, 2021), pp. 1–3.
- [15] P. C. Jamison, T. Tsunoda, T. A. Vo, J. Li, H. Jagannathan, S. R. Shinde, V. K. Paruchuri, and D. Gall, *IEEE Trans. Electron Devices* **62**, 2878 (2015).
- [16] R. Rosenberg, D. Edelstein, C.-K. Hu, and K. Rodbell, *Annu. Rev. Mater. Res.* **30**, 229 (2000).
- [17] T. Nogami, O. Gluschenkov, Y. Sulehria, S. Nguyen, B. Peethala, H. Huang, H. Shobha, N. Lanzillo, R. Patlolla, D. Sil *et al.*, in *Proceedings of the 2022 IEEE Symposium on VLSI Technology and Circuits (VLSI Technology and Circuits)* (IEEE, Piscataway, NJ, 2022), pp. 423–424.
- [18] M. Ashby and A. Greer, *Scr. Mater.* **54**, 321 (2006).
- [19] W. Wang, *Adv. Mater.* **21**, 4524 (2009).
- [20] P. K. Gupta and W. Kob, *J. Non-Cryst. Solids* **3**, 100031 (2019).
- [21] Y. Qiu, L. W. Antony, J. J. de Pablo, and M. D. Ediger, *J. Am. Chem. Soc.* **138**, 11282 (2016).
- [22] K. J. Dawson, K. L. Kearns, M. D. Ediger, M. J. Sacchetti, and G. D. Zografis, *J. Phys. Chem. B* **113**, 2422 (2009).
- [23] R. C. Bell, H. Wang, M. J. Iedema, and J. P. Cowin, *J. Am. Chem. Soc.* **125**, 5176 (2003).
- [24] C. J. Ellison and J. M. Torkelson, *Nat. Mater.* **2**, 695 (2003).
- [25] D. R. Reid, I. Lyubimov, M. Ediger, and J. J. De Pablo, *Nat. Commun.* **7**, 13062 (2016).
- [26] J. D. Stevenson and P. G. Wolynes, *J. Chem. Phys.* **129**, 234514 (2008).
- [27] S. Samanta, G. Huang, G. Gao, Y. Zhang, A. Zhang, S. Wolf, C. N. Woods, Y. Jin, P. J. Walsh, and Z. Fakhraai, *J. Phys. Chem. B* **123**, 4108 (2019).
- [28] S. Torquato and F. H. Stillinger, *Phys. Rev. E* **68**, 041113 (2003).
- [29] R. Xie, G. G. Long, S. J. Weigand, S. C. Moss, T. Carvalho, S. Roorda, M. Hejna, S. Torquato, and P. J. Steinhardt, *Proc. Natl. Acad. Sci. U.S.A.* **110**, 13250 (2013).
- [30] F. Martelli, S. Torquato, N. Giovambattista, and R. Car, *Phys. Rev. Lett.* **119**, 136002 (2017).
- [31] L. Berthier and G. Tarjus, *Phys. Rev. E* **82**, 031502 (2010).
- [32] M. Leocmach, J. Russo, and H. Tanaka, *J. Chem. Phys.* **138**, 12A536 (2013).
- [33] C. P. Royall, F. Turci, S. Tatsumi, J. Russo, and J. Robinson, *J. Phys. Condens. Matter* **30**, 363001 (2018).
- [34] H. Tanaka, H. Tong, R. Shi, and J. Russo, *Nat. Rev. Phys.* **1**, 333 (2019).
- [35] F. Martelli, F. Leoni, F. Sciortino, and J. Russo, *J. Chem. Phys.* **153**, 104503 (2020).
- [36] S. Singh, M. D. Ediger, and J. J. De Pablo, *Nat. Mater.* **12**, 139 (2013).
- [37] F. Martelli, H.-Y. Ko, E. C. Oğuz, and R. Car, *Phys. Rev. B* **97**, 064105 (2018).
- [38] F. Martelli, N. Giovambattista, S. Torquato, and R. Car, *Phys. Rev. Mater.* **2**, 075601 (2018).
- [39] T. Jenkinson, P. Crowther, F. Turci, and C. P. Royall, *J. Chem. Phys.* **147**, 054501 (2017).
- [40] C. Patrick Royall, S. R. Williams, T. Ohtsuka, and H. Tanaka, *Nat. Mater.* **7**, 556 (2008).
- [41] M. Leocmach and H. Tanaka, *Nat. Commun.* **3**, 974 (2012).
- [42] C. P. Royall and S. R. Williams, *Phys. Rep.* **560**, 1 (2015).
- [43] S. S. Dalal and M. D. Ediger, *J. Phys. Chem. Lett.* **3**, 1229 (2012).
- [44] See Supplemental Material at <http://link.aps.org/supplemental/10.1103/PhysRevLett.130.198201> for details on simulations, which includes Refs. [45–47].
- [45] Z. Shi, P. G. Debenedetti, and F. H. Stillinger, *J. Chem. Phys.* **134**, 114524 (2011).
- [46] E. A. A. Pogna, C. Rodríguez-Tinoco, G. Cerullo, C. Ferrante, J. Rodríguez-Viejo, and T. Scopigno, *Proc. Natl. Acad. Sci. U.S.A.* **112**, 2331 (2015).
- [47] L. Berthier and M. D. Ediger, *J. Chem. Phys.* **153**, 044501 (2020).

- [48] G. Wahnström, *Phys. Rev. A* **44**, 3752 (1991).
- [49] A. Malins, S. R. Williams, J. Eggers, and C. P. Royall, *J. Chem. Phys.* **139**, 234506 (2013).
- [50] D. Coslovich and G. Pastore, *J. Chem. Phys.* **127**, 124504 (2007).
- [51] U. R. Pedersen, T. B. Schröder, J. C. Dyre, and P. Harrowell, *Phys. Rev. Lett.* **104**, 105701 (2010).
- [52] A. P. Thompson, H. M. Aktulga, R. Berger, D. S. Bolintineanu, W. M. Brown, P. S. Crozier, P. J. in 't Veld, A. Kohlmeyer, S. G. Moore, T. D. Nguyen, R. Shan, M. J. Stevens, J. Tranchida, C. Trott, and S. J. Plimpton, *Comput. Phys. Commun.* **271**, 108171 (2022).
- [53] A. Stukowski, *Model. Simul. Mater. Sci. Eng.* **18**, 015012 (2009).
- [54] S. S. Dalal, Z. Fakhraai, and M. D. Ediger, *J. Phys. Chem. B* **117**, 15415 (2013).
- [55] C. J. Fullerton and L. Berthier, *Europhys. Lett.* **119**, 36003 (2017).
- [56] A. Sepúlveda, M. Tylinski, A. Guiseppi-Elie, R. Richert, and M. D. Ediger, *Phys. Rev. Lett.* **113**, 045901 (2014).
- [57] K. R. Whitaker, M. Tylinski, M. Ahrenberg, C. Schick, and M. D. Ediger, *J. Chem. Phys.* **143**, 084511 (2015).
- [58] W. Kob and H. C. Andersen, *Phys. Rev. Lett.* **73**, 1376 (1994).
- [59] F. C. Frank and J. S. Kasper, *Acta Crystallogr.* **11**, 184 (1958).
- [60] M. Godonoga, A. Malins, J. Eggers, and C. P. Royall, *Mol. Phys.* **109**, 1393 (2011).
- [61] A. R. Moore, G. Huang, S. Wolf, P. J. Walsh, Z. Fakhraai, and R. A. Riggelman, *Proc. Natl. Acad. Sci. U.S.A.* **116**, 5937 (2019).
- [62] A. Zhang, A. R. Moore, H. Zhao, S. Govind, S. E. Wolf, Y. Jin, P. J. Walsh, R. A. Riggelman, and Z. Fakhraai, *J. Chem. Phys.* **156**, 244703 (2022).